Electrochimica Acta 212 (2016) 686–693

Contents lists available at ScienceDirect

Electrochimica Acta

journal homepage: www.elsevier.com/locate/electacta

Ultrafine Iridium Oxide Nanorods Synthesized by Molten Salt Method toward Electrocatalytic Oxygen and Hydrogen Evolution Reactions

Jahangeer Ahmed[1], Yuanbing Mao*

Department of Chemistry, University of Texas Rio Grande Valley, 1201 West University Drive, Edinburg, Texas 78539, USA

ARTICLE INFO

Article history:
Received 14 February 2016
Received in revised form 21 June 2016
Accepted 23 June 2016
Available online 1 July 2016

Keywords:
IrO_2
nanorods
molten salt synthesis
oxygen evolution reaction (OER)
hydrogen evolution reaction (HER)

ABSTRACT

Ultrafine iridium oxide nanorods (IrO_2 NRs) were successfully synthesized using a molten salt method at 650 °C. The structural and morphological characterizations of these IrO_2 NRs were carried out by powder X-ray diffraction, Raman spectroscopy and electron microscopic techniques. Compared to commercial IrO_2 nanoparticles (IrO_2 NPs) and previous reports, these IrO_2 NRs show enhanced electrocatalytic activity to oxygen and hydrogen evolution reactions by passing either N_2 or O_2 gas in a 0.5 M KOH electrolyte before electrochemical measurements, including cyclic voltammetry, chronoamperometry and electrochemical impedance spectroscopy. Specifically, the current densities from the as-synthesized IrO_2 NRs and commercial IrO_2 NPs were measured in 0.5 M KOH electrolyte to be 70 and 58 (OER, deaerated, at 0.6 V versus Ag/AgCl), 71 and 61 (OER, O_2, from −0.10 to 1.0 V versus Ag/AgCl at 50 mV/s), and 25 and 14 (HER, deaerated, at −1.4 V versus Ag/AgCl) mA/cm^2, respectively. These results are comparable with, and in most cases, higher than reported data in the literature. Therefore, the current study reports not only a novel synthetic process for IrO_2 but also a high efficient IrO_2 nanostructure, and it is expected that these IrO_2 NRs can serve as a benchmark in the development of active OER and HER (photo)electrocatalysts for various applications.

1. Introduction

The storage of renewable energy using hydrogen "fuel" has been viewed as a viable mechanism by electrolysis of water into oxygen and hydrogen fuels, but is hampered by the slow kinetics of the oxygen evolution reaction (OER). Hence there is a broad effort to improve performance of currently used materials and develop new materials. Iridium oxide (IrO_2) is an effective stable electro-catalyst which can lower the over-potential and keep a remarkable current to improve the efficiency of fuel generation technologies [1,2]. Nanostructured IrO_2 materials have been highlighted as the most promising electrode materials to enhance the electrocatalytic activity in both OER and hydrogen evolution reaction (HER) from the photo-electrochemical water-splitting and electrolysis [3,4,5,6,7,8]. Nanocrystalline IrO_2 and RuO_2 are recognized to be the best electrocatalysts for HER and OER in both acidic and alkaline media even though a growing body of OER and HER catalysts containing abundant, inexpensive transition metals and their oxides have recently appeared in the literature [9,10]. The continuous use of relatively expensive materials by industry is because the economics of electrolytic hydrogen production are governed mainly by catalytic performance rather than the catalyst cost and earth-abundant materials are typical not as stable [11]. Recently, Stoerzinger et al. have reported the surface orientated oxygen evolution activities of IrO_2 and RuO_2 in O_2-saturated 0.1 M KOH electrolyte at 1.53 V versus reversible hydrogen electrode [12]. The potentials range of IrO_2 electrocatalysts for OER were reported from 0.77 V to 1.5 V using acidic and alkaline solutions as the electrolytes [7,10,13,14,15,16,17,18,19]. The lowest potential of IrO_2 nanostructures was reported of 0.77 V for the OER in 0.1 M phosphate buffer solution using ITO electrode [13].

IrO_2 nanostructures have also been used widely as the electrocatalysts for the OER in proton exchange membrane (PEM) water electrolysis [15,16,20], solid polymer electrolyte (SPE) electrolyzer [13,17], photocatalytic and electrolysis of water oxidation, etc [3,6,8,13]. IrO_2 nanostructures were also used as the electrocatalysts in the oxygen reduction [1], oxidation of carbon mono-oxide, methanol and ethanol, etc [21,22]. Apart from the electrocatalysis, IrO_2 nanostructures were also used in several other applications including sensing [23], field emission [24,25], Li-air battery [26], electrical properties, etc [27].

* Corresponding author. Tel.: +1 956 665 2417.
E-mail address: yuanbing.mao@utrgv.edu (Y. Mao).
[1] Current address: Department of Chemistry, College of Science, King Saud University, Riyadh 11451, Saudi Arabia.

http://dx.doi.org/10.1016/j.electacta.2016.06.122
0013-4686/

IrO_2 nanostructured materials were mostly synthesized by metal organic chemical vapor deposition (MOCVD) method [23,28,29,30,31,32,33,34,25]. A variety of IrO_2 nanostructures have also been produced by various other techniques, including vapor phase transport process [35], electrochemical synthesis [13], arc vaporization [36], hydrothermal [4], reactive radio frequency magnetron sputtering (RFMS) [37], sol–gel [38,39], wetness method [9], Adams fusion method [15,16], sulfite complex route [14], thermal decomposition of precursor (H_2IrCl_6) [17], oleylamine-mediated synthesis, etc [10]. With a closer look, it can be found that many of these methods employ expensive, complex, unstable and not-environmentally-friendly iridium-containing precursors followed with tedious synthetic procedure in complicated experimental setups. Molten salt synthesis process is the cost effective, stable and eco-friendly method compared to above reported methods. This method has also been employed earlier as a simple and facile approach in the synthesis of various nanostructured materials [40,41,42]. Herein, we report the successful synthesis of IrO_2 nanorods with an average diameter of ~15 nm and length of ~200 nm for the first time using iridium tetrachloride as precursor in a molten salt of sodium chloride and potassium chloride mixture at 650 °C for 12 h in ambient air atmosphere. The structural and morphological characterizations of IrO_2 NRs were investigated by powder X-ray diffraction (PXRD), Raman spectroscopy, energy dispersive X-ray studies, single point BET surface area measurements and electron microscopic studies. Note that an effective electrocatalyst can lower the over-potential to sustain the current and, therefore, to improve the efficiency of an electrocatalyst toward the gas evolution reactions due to loss of minimum energy in the electrochemical reactions. Electrocatalytic studies of the IrO_2 NRs toward OER and HER have been investigated by cyclic voltammetry (CV) and chronoamperometry (CA) in alkaline 0.5 M KOH aqueous electrolyte versus Ag/AgCl electrode, and obtained results were compared to commercial IrO_2 NPs and previously reported work.

2. Experimental

2.1. Materials and method

The following reagents were used in the synthesis of the IrO_2 NRs by the molten salt process: $IrCl_4$ (Alfa Aesar, 99.95%), NaCl (Alfa Aesar, 99.0%), and KCl (Sigma Aldrich, 99.0%). The precursors were taken with the molar ratio of 1:30:30 of $IrCl_4$:NaCl:KCl and ground together in an agate mortar pestle for 20 minutes. The resulting mixture was transferred to a covered rectangular crucible and kept at 650 °C for 12 h in a programmable high temperature furnace with the heating and cooling rate of 5 °C/minute in air. The resulting products were washed with de-ionized water several times and then dried at 60 °C for 6 h in oven. Commercial IrO_2 nanoparticles (NPs) from Sigma Aldrich (99.9%) were used to compare the electrocatalytic activity with the as-synthesized IrO_2 NRs.

2.2. Characterizations

The resulting fine black colored powder of the IrO_2 NRs was characterized initially by PXRD on a Rigaku MiniFlex X-ray diffractometer using Ni-filtered Cu-Kα radiation. Diffraction patterns were recorded with a step size and scan speed of 0.01° and 1 s, respectively, on an aluminum sample holder. Raman scattering data was recorded by employing the back-scattering geometries on a Bruker SENTERRA RAMAN microscope with an objective of 20X optical microscope. The excitation line (785 nm) of an Ar+ laser beam was focused to a spot size of 5 μm with a laser power of 25 mW. The used spectral resolution range was 3–5 cm^{-1} with the integration time of 100 s. Field emission SEM study was carried out with a ZEISS SIGMA VP electron microscope operated at 5 kV. Transmission electron microscopy (TEM), high resolution TEM (HRTEM), and selected area electron diffraction (SAED) analyses were carried out with a Hitachi H-9500 electron microscope operated at 300 kV. The samples for TEM studies were prepared by dispersing the IrO_2 NRs in ethanol via utrasonic process for 5 minutes, and a drop of the formed suspension was put onto a carbon coated copper grid, and then dried in air. Surface area analysis was performed on a Micromeritics ASAP 2020 Surface Area and Porosity Analyzer with nitrogen at cryogenic temperature (77.3 K).

2.3. Preparation of electrode materials and electrochemical measurements

The working electrode was modified with the as-synthesized IrO_2 NRs for the electrochemical studies toward OER and HER. The IrO_2 nanostructures modified electrodes were prepared by mixing the nanopowder, carbon black and PVDF. The powder of IrO_2 NRs was ground with carbon black and PVDF in the weight fraction of 75:15:10, with a small amount of ethanol and then pasted on the glassy carbon electrode. The prepared electrode materials were then dried overnight at 65 °C in vacuum oven. The electrochemical

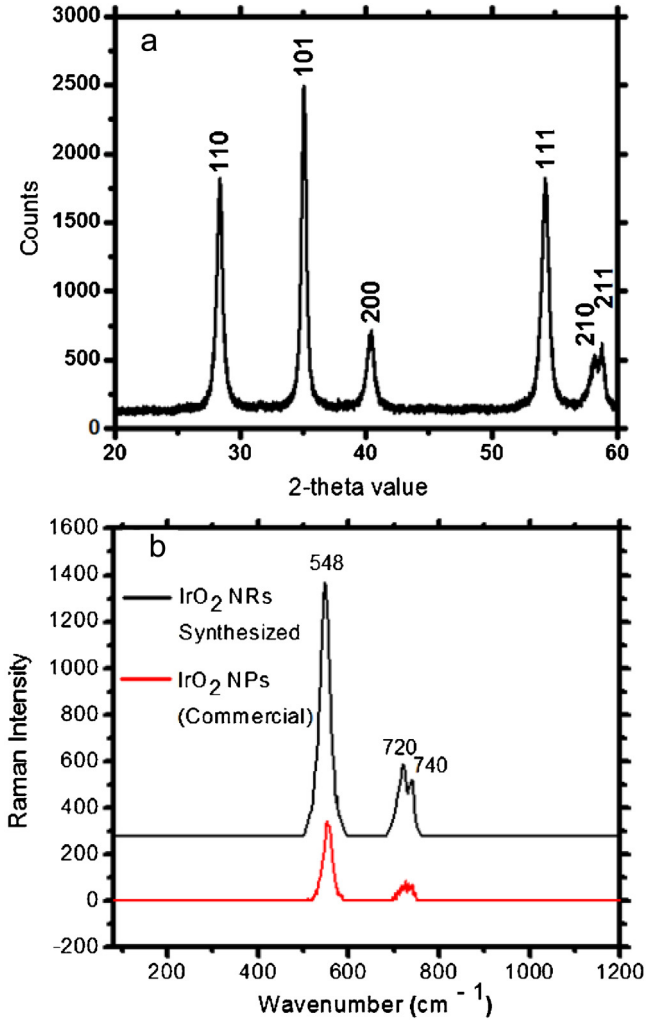

Fig. 1. (a) Powder x-ray diffraction pattern of the IrO_2 NRs synthesized by the molten salt process at 650 °C for 12 h. (b) Raman spectra of the IrO_2 NRs and commercial IrO_2 NPs.

studies were carried out with a potentiostat/galvanostat electrochemical work station (Metrohm Autolab B.V.) at room temperature. The electrochemical work station contains three electrodes including the IrO_2 NRs coated glassy carbon as the working electrode, Ag/AgCl as the reference electrode and a Pt wire as the counter electrode. CV measurements were carried out at different scan rates of 100, 50, 20 and 10 mV/s with a peak window between 0 and −1.4 V versus the Ag/AgCl electrode for the HER and from 0 to 1.0 V versus the Ag/AgCl electrode for the OER. CA characterization was carried out for 200 s at various fixed potentials versus the Ag/AgCl electrode for HER (at −1.4, − 1.2, − 1.0 and −0.9 V) and OER (at 0.60, 0.65, 0.70 and 0.75 V). CV and CA measurements were carried out in an alkaline electrolyte of 0.5 M KOH aqueous solution. Prior to the electrochemical measurements, nitrogen gas was flown through the electrolyte solution for 5 minutes to remove dissolved air from the electrolyte. Also, electrochemical measurements were run in 0.5 M KOH solution saturated with O_2 toward the OER. Note that freshly prepared electrodes and electrolytes were used in each measurement and the current density of the IrO_2 electrocatalysts was calculated using the geometric electro-active surface area of electrode from Randles–Sevcik equation [43,44,45]. Also note that the geometric electro-active surface area of freshly prepared electrodes could vary due to the variation of amount of pasted materials on fresh glassy carbon electrode. Electrochemical impedance spectroscopic (EIS) studies were also carried in three electrode configuration using the same Metrohm Autolab electrochemical work station with the frequency ranging from 100 mHz to 100 kHz at 1.0 V in 0.5 M KOH solution.

3. Results and discussion

The phase purity of our as-synthesized IrO_2 NRs was characterized by PXRD and Raman spectroscopy. The observed reflections from the synthesized IrO_2 NRs (Fig. 1a) could be perfectly indexed with the peaks of (110), (101), (200), (111), (210) and (211) on the basis of rutile phase IrO_2 with tetragonal crystal structure (JCPDS file # 88-0288). The relative strong intensity of the (101) peak is an evidence of the orientation of the ⟨101⟩ plane of rutile phase of the IrO_2 NRs. As detected by PXRD, the commercial IrO_2 NPs (Sigma Aldrich, 99.9%) were amorphous in nature. In addition to XRD data, evidence regarding the chemical composition of the IrO_2 nanomaterials was obtained from Raman spectroscopy. Three characteristic Raman bands (Fig. 1b) are identified at 548, 720 and 740 cm^{-1} from the IrO_2 NRs and commercial IrO_2 NPs. Well correlated with those of IrO_2 nanocrystals, these bands can be correspondingly assigned to the first order E_g,B_{2g}, and A_{1g} phonon bands of rutile IrO_2 structure, respectively [37].

Field emission SEM (FESEM) images (Fig. 2a–c) of the as-synthesized IrO_2 product confirm the formation of ultrafine nanorods, appearing in rectangular shape with the diameter ranging from 8 nm to 20 nm and an average diameter of 15 nm. Energy dispersive studies (Inset of Fig. 2a) confirmed that our as-synthesized IrO_2 NRs only contain iridium and oxygen elements with no other impurities, which clearly support the PXRD and Raman data from the IrO_2 NRs (Fig. 1). FESEM image of the commercial IrO_2 NPs shows the spherical shape with an average size of ∼60 nm (Fig. 2d).

TEM and HRTEM studies (Fig. 3) were employed to characterize the morphology, size and crystalline behavior of the resulting IrO_2 NRs. TEM image (Fig. 3a) confirms the formation of IrO_2 NRs with the average diameter and length of ∼15 nm and ∼200 nm, respectively. HRTEM image shows a lattice spacing value of 3.20 Å, which is consistent with (110) plane of IrO_2 NRs (Fig. 3b). Electron diffraction (ED) pattern of the IrO_2 NRs shows the circular fashion of the spots due to (110), (101), (200), (210), (211), and (220) planes which indicate the formation of tetragonal crystal structure of IrO_2 NRs (Fig. 3c). Both the HRTEM image and ED pattern confirm the crystalline behavior of the IrO_2 NRs.

Molten salt synthetic process (i.e. using chlorides as the salts) is a significant approach to synthesize a wide variety of materials with high crystallinity, including the formation of nanospheres,

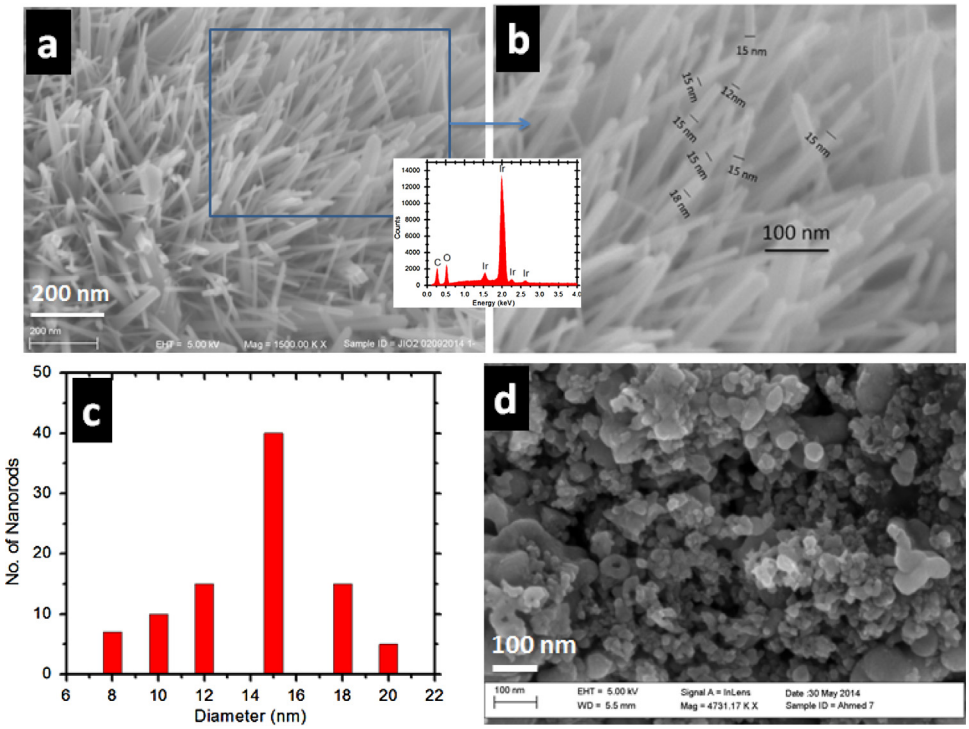

Fig. 2. (a & b) FESEM images of the IrO_2 NRs. The inset shows the corresponding energy dispersive X-ray spectrum. (c) Size distribution of the IrO_2 NRs with respect to the diameters. (d) FESEM image of the commercial IrO_2 NPs.

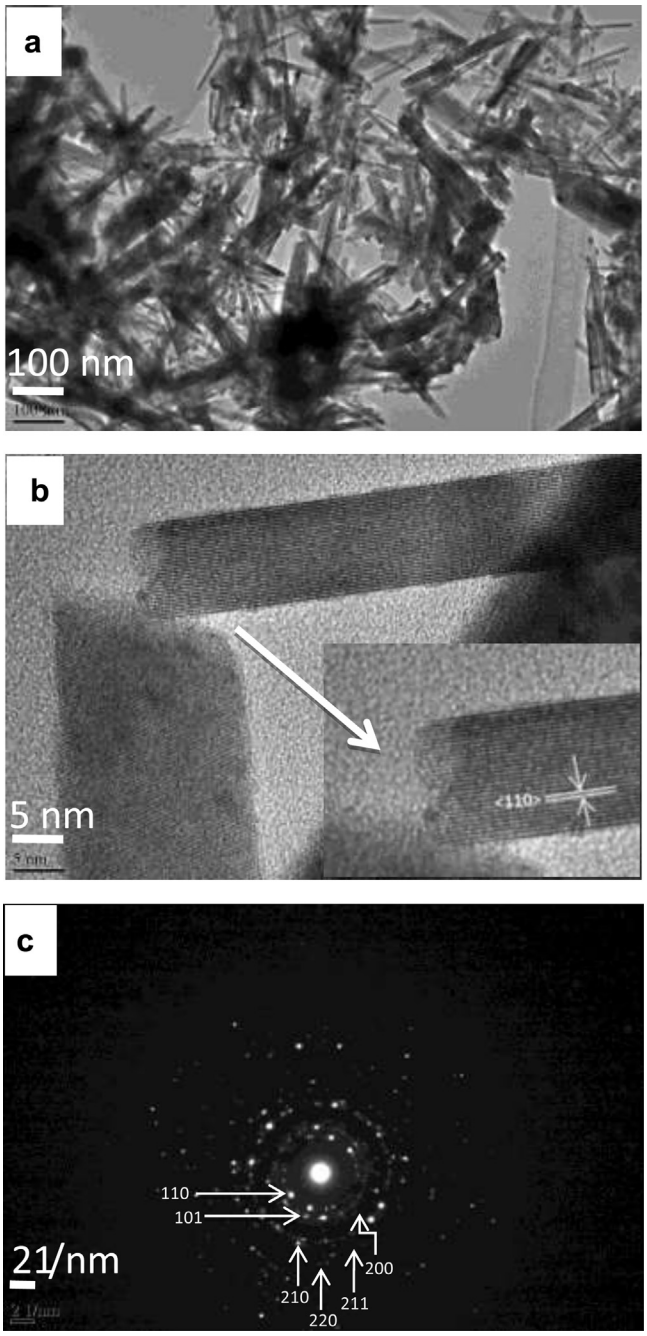

Fig. 3. (a) Typical TEM image of the IrO_2 NRs (scale bar = 100 nm). (b) Representative HRTEM image of the IrO_2 NRs (scale bar = 5 nm). (c) Electron diffraction pattern of the IrO_2 NRs.

nanocubes, and nanorods. The surface and interface energies between the transition metal precursors and the molten salts minimize the activation energies to form unusual morphologies of products [46]. The morphology of the nanomaterials in molten salts could be influenced by various parameters including precursors, synthetic conditions, nature of the salts, diffusion of the salts, and the solubility of the constituents [46,47]. Recently Rørvik et al. had reported that the sodium chloride plays a crucial role in the growth of nanorods of ternary oxides in the molten salt synthesis while no rod shaped morphology was observed without sodium chloride [47]. We observed similar phenomena here from the synthesis of the IrO_2 NRs with the chloride mixture as the molten salt. The molten salt method had also been used earlier in the synthesis of nanorods of other binary [48,49], and ternary oxides [47,50,51], but it is the first time for IrO_2 as reported in this manuscript.

Electrochemical stability and gas evolution activity of the iridium oxides electrocatalysts depend on the chemical and structural nature as well as the size and morphology of the materials and their synthetic conditions [19,52]. Crystalline metal oxides are electrochemically more stable compared to amorphous oxides materials for the gas evolution reactions [19]. However if amorphous IrO_2 nanoparticles were calcined at high temperature (>550 °C) then it could cause the agglomeration of the nanoparticles which may lead to increase their particle size. Therefore, calcined commercial IrO_2 nanoparticles would not show enhancement of their electrochemical activity towards the OER and HER due to larger particle size. The electrochemical CV and CA measurements were carried out to evaluate the electrocatalytic activity of the IrO_2 NRs and commercial IrO_2 NPs toward OER and HER. Fig. 4a shows the cyclic voltammograms of the IrO_2 NRs with a peak window from 0 to 1.0 V versus Ag/AgCl with scan rates of 100, 50, 20 and 10 mV/s to study their redox behaviors. The peak observed at ~0.55 V could be due to the transformation of Ir^{3+} to Ir^{4+} [10,11]. Noticeably, the electrocatalytic oxidation current was observed beyond this potential in the cyclic voltametric curves due to the following reaction occurs at the electrode surface: $4OH^- \rightarrow 2H_2O + 2O_2 + 4e^-$. IrO_2 NPs supported on glassy carbon electrode were also employed for the OER in acidic (0.1 M $HClO_4$) and alkaline (0.1 M KOH) solutions at 1.5 V versus reversible hydrogen electrode (RHE) by using a rotating ring disc electrode [10]. So far, the lowest potential of IrO_2 nanostructures for the OER was reported of 0.77 V using the ITO electrode from 0 to 1.4 V versus Ag/AgCl at a scan rate of 20 mVs^{-1} in 0.1 M phosphate buffer solution [13]. Herein, this is noteworthy that the OER starts at a much lower potential using our IrO_2 NRs compared to previous reports [10,13].

Chronoamperometry is a potentiostatic experiment and true quantitative measurements to study the electro-catalytic activity of the materials with three electrode systems at the fixed potential with time. It is important to use less energy for current generation and to find optimal oxygen generating electrocatalysts to minimize the energy loss. Previously, current densities of IrO_2 nanostructures were reported of 10 mA/cm^2 at 1.7 V vs $Hg/Hg_2SO_4/K_2SO_4$ in 0.1 M KOH and 0.1 M $HClO_4$ and 30 mA/cm^2 at 1.5 V vs $Hg/Hg_2SO_4/K_2SO_4$ in 0.1 M H_2SO_4 on the literature [10,53]. IrO_2 nanostructures as the electrocatalysts generate a very high current (100 mA/cm^2–1.7 A/cm^2) using PEM and SPE water electrolysis at 1.8 V [14,16,17]. Herein, Fig. 4b shows chronoamperometric measurements of the IrO_2 NRs supported on glassy carbon electrode at the fixed potentials varied from 0.6 V to 0.75. In our experiment, when the potential is switched off then the electrochemical reaction stops and hence current drops drastically. We also observed that the erosion of the materials (from the working electrode) occurred at the higher voltage during OER. Using Randles–Sevcik equation and the geometric electro-active surface area (0.70 cm^2) of the IrO_2 NR coated electrode, the current densities were found to be 86, 82, 78 and 70 mA/cm^2 at the potentials of 0.60, 0.65, 0.70 and 0.75 V, respectively [43,44,45]. Therefore, even our synthesis method to make these IrO_2 NRs is very facile and cost-efficient using simple precursor, the obtained OER current densities could be comparable with and even higher than what previously have been reported in the literature. Fig. 4c shows the cyclic voltammograms of the commercial IrO_2 NPs with a peak window from −1.4 to 1.2 V versus Ag/AgCl with scan rates of 200, 50, and 25 mV/s. In CV, an anodic sweep corresponds to the scan towards the positive potential while cathodic sweep denotes the scan towards the negative potential. By comparing the voltammograms from the as-synthesized IrO_2 NRs with those

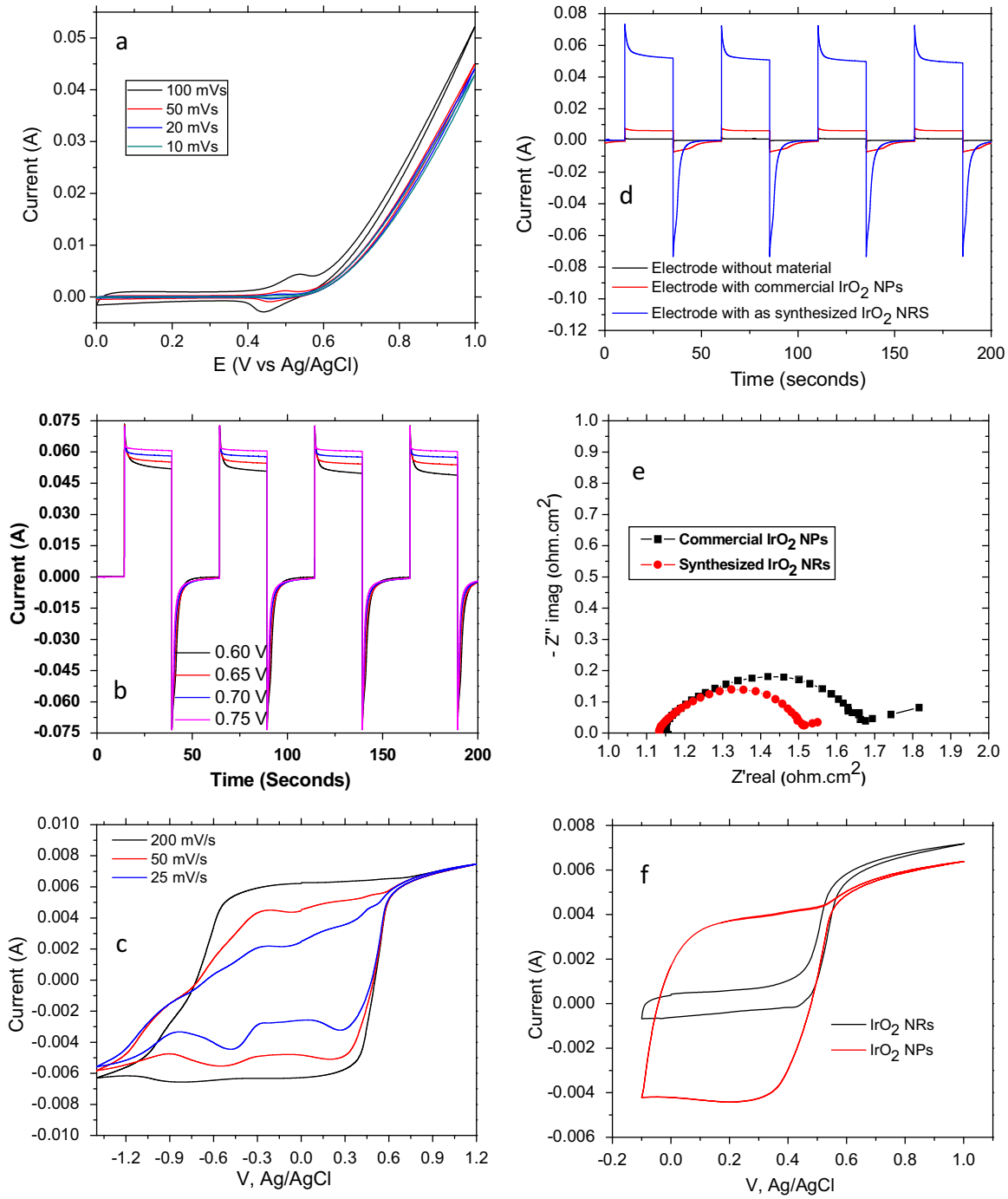

Fig. 4. (a) CV and (b) chronoamperometric studies of the IrO_2 NRs for OER in 0.5 M KOH deaerated aqueous solution. (c) CV of the commercial IrO_2 NPs in 0.5 M KOH deaerated aqueous solution. (d) Comparative chronoamperometric voltammograms of the as-synthesized IrO_2 NRs and commercial IrO_2 NPs for OER at 0.6 V versus Ag/AgCl. (e) EIS of the as-synthesized IrO_2 NRs and commercial IrO_2 NPs. (f) CV of the IrO_2 NRs and commercial IrO_2 NPs for OER in 0.5 M KOH aqueous solution saturated with O_2 at the scan rate of 50 mV/s.

from commercial IrO_2 NPs for OER, we clearly observe that the IrO_2 NRs show superior electrocatalytic activity over the commercial IrO_2 NPs toward the OER in 0.5 M KOH solution at 0.6 V versus Ag/AgCl electrode (Fig. 4a and c).

Fig. 4d shows the chronoamperometric voltammogram of the three electrodes coated by the IrO_2 NRs, commercial IrO_2 NPs and no materials. The as-synthesized IrO_2 NRs generate higher current density (70 mA/cm^2, calculated by using the geometric electroactive surface area of electrode of 0.70 cm^2) than the commercial IrO_2 NPs (58 mA/cm^2, calculated by using the geometric electroactive surface area of electrode of 0.12 cm^2) at 0.6 V versus Ag/AgCl electrode. The chronoamperometry to the current generation depends on many aspects of electrocatalytic-active materials. For example, the dependence of electro-catalytic activity on morphological and orientation of nanostructured materials has been reported [12,54]. Similarly, for IrO_2 nanostructures, the generated current density depends on both the surface area and morphology as a conjunction of both faradaic and non-faradaic processes. In the faradaic process, charges being transferred across the electrode-electrolyte interface are governed by the Faraday's law, and electrons transferred from the IrO_2 atoms to water molecules to generate hydroxide ions and hydrogen molecules as OER and HER,

respectively. For the non-faradaic process, only the formation of the electrical double layer is motivated. From electron microscopic measurements (Figs. 2 and 3), the diameter and length of the as-synthesized IrO_2 NRs were found to be ~15 nm and ~200 nm, respectively, and the diameter of the commercial IrO_2 NPs was ~60 nm. The surface area of the IrO_2 NRs and commercial IrO_2 NPs was measured by single point BET and found to be ~14 m^2/g and ~12 m^2/g, respectively. As expected, the surface area increases with decreasing grain size of the IrO_2 nanostructures. However, other than difference on surface area, different crystallinity (rutile crystal phase *vs* amorphous phase, Fig. 1) and morphology (nanorod *vs* nanoparticle) may also play important roles on the variation of OER current density between the IrO_2 NRs and commercial IrO_2 NPs. Further investigation is needed on these aspects in the future.

Fig. 4e shows EIS spectra of the IrO_2 NRs and commercial IrO_2 NPs in 0.5 M KOH solution. The collected Nyquist plots of the Z′ real *vs* negative Z″ imaginary at 1.0 V vs Ag/AgCl show the observed impedance semicircles from both electrode materials. The ohmic resistance of charge transfer (R_{ct}) of the IrO_2 NRs was found to be ~0.35 ohm·cm^2, lower than that of the commercial IrO_2 NPs (R_{ct} = ~0.52 ohm·cm^2) and similar with that of the reported Pt/IrO_2 electrocatalyst [2]. Both the Faradic reactions and electrical double-layer on the electrode surface are represented by R_{ct}. The impedance response, governed by the faradic gas evolutions, supports the enhanced electrocatalytic activity of IrO_2 NRs over the commercial IrO_2 NPs.

The oxygen evolution activity of IrO_2 electrocatalysts has also been carried out in 0.5 M KOH aqueous solution saturated with O_2 gas. Similarly freshly prepared electrodes and electrolyte solutions were used in three electrode system, but O_2 gas flowed for 30 min before starting CV experiments. The cyclic voltammograms of the IrO_2 nanostructures were collected by applying potential ranging from −0.10 to 1.0 V versus Ag/AgCl electrode at the scan rate of 50 mV/s (Fig. 4f). From the CV curves, it can be easily observed that the IrO_2 NRs generate higher current compared to the IrO_2 NPs. The current density of freshly prepared electrodes containing IrO_2 NRs (geometric electroactive surface area of electrode = 0.10 cm^2) and IrO_2 NPs (geometric electroactive surface area of electrode = 0.30 cm^2) were found to be 71 mA/cm^2 and 61 mA/cm^2, respectively. These results are consistent with those measured in deaerated electrolyte, and that the electrocatalytic activity of the as-synthesized IrO_2 NRs is higher than the commercial and many previously reported IrO_2 electrocatalysts.

Previously, IrO_2 nanostructured materials have been used as an electrocatalyst with SPE in HER [9]. Meanwhile, hydrogen has been proposed as a potential replacement for our rapidly depleting fossil fuel resources [55]. Boodts and Trasatti were reported two decades ago that IrO_2 is a good electrocatalyst for HER and shown the current density in the order of 10^{-3} A/cm^2 [56]. Cheng et al. had reported that carbon supported IrO_2 and RuO_2 generated current density in the range from 10^{-6} to 10^{-3} A/cm^2 with the scan window from −0.3 to 0.3 V using 0.5 M H_2SO_4 as an electrolyte [9]. Therefore, HER performance of the IrO_2 NRs was also evaluated by applying a negative potential versus Ag/AgCl electrode. Fig. 5a shows the CV curves of freshly prepared IrO_2 NR electrodes in deaerated 0.5 M KOH solution by nitrogen gas for 5 min by scanning with different rates of 100, 50, 20 and 10 mV/s from 0 to −1.4 V versus Ag/AgCl electrode. It was observed that HERs started from −0.80 V on the surface of working electrode containing the IrO_2 NRs versus Ag/AgCl according to the following reaction: $2H_2O + 2e^- \rightarrow H_2 + 2OH^-$. Chronoamperometric studies of IrO_2 NRs were also carried out for HER over the surface of IrO_2 electrode in 0.5 M KOH at fixed potentials with time (Fig. 5b). The current densities from the chronoamperometric measurements using the electroactive surface area of electrode (0.35 cm^2) for HER were

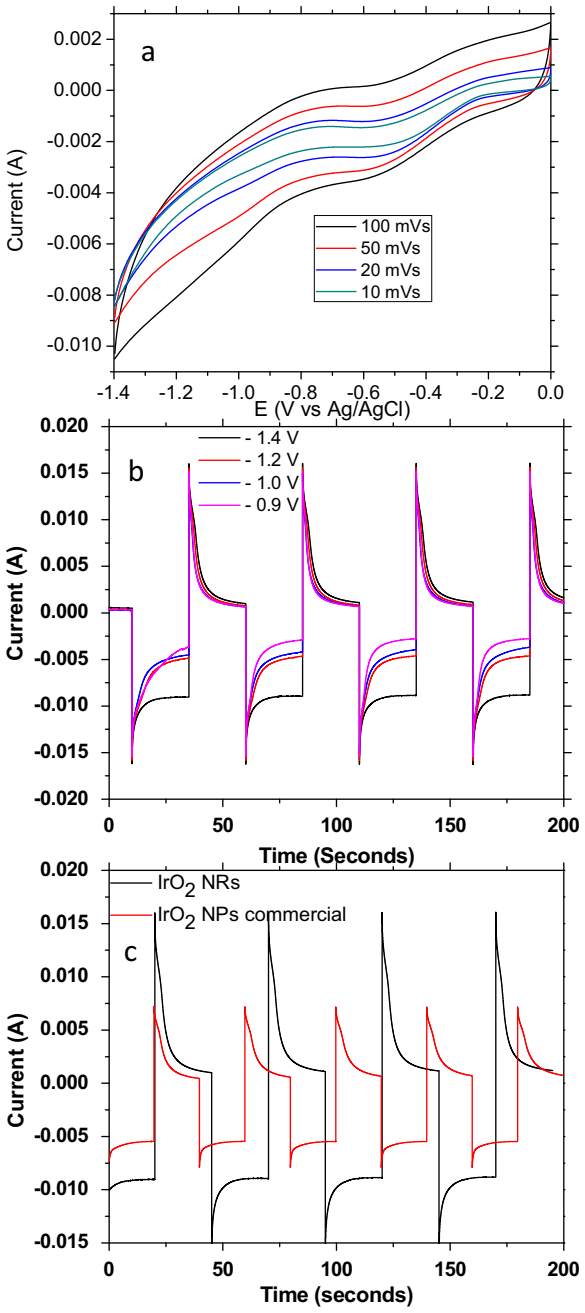

Fig. 5. (a) Cyclic voltammetry and (b) chronoamperometry of the IrO_2 NRs for HER in deaerated 0.5 M KOH. (c) Comparative chronoamperometric voltammograms of the as-synthesized IrO_2 NRs and commercial IrO_2 NPs for HER at −1.4 V versus Ag/AgCl electrode in 0.5 M KOH.

found to be 8, 12, 14 and 25 mA/cm^2 at the potentials of −0.90, −1.00, −1.20 and −1.40 V, respectively. The generated cathodic current is directly proportional to the rate of hydrogen evolution, so the higher currents generated at −1.4 V may be due to higher electron transfer rate from electrolyte to the electrode surface compared to those at −0.90, −1.00, −1.20 V. These results are comparable with and even higher than literature results, even direct comparison should be done with caution due to different measurement conditions [9,56]. Fig. 5c shows the comparative chronoamperometric studies of the IrO_2 NRs and commercial IrO_2 NPs at −1.4 V versus Ag/AgCl electrode in 0.5 M KOH electrolyte. For HER, the current density of the IrO_2 NRs (25 mA/cm^2) was

found to be nearly double to that of the commercial IrO_2 NPs (14 mA/cm^2). Therefore, the IrO_2 NRs show enhanced electrocatalytic HER activity and enhanced OER activity, as discussed above, compared to the commercial IrO_2 NPs and other reported work.

4. Conclusions

In this paper, we report the successful synthesis of ultrafine IrO_2 nanorods with average diameter and length of 15 nm and 200 nm, respectively, using a facile molten salt method at 650 °C in air. These IrO_2 NRs possess enhanced electrocatalytic OER and HER activities compared to the commercial IrO_2 nanoparticles after passing either N_2 or O_2 gas into the electrolyte before experiments, as confirmed by cyclic voltammetry and chronoamperometric measurements and supported by electrochemical impedance spectroscopic studies. Specifically, the as-synthesized IrO_2 NRs generate higher OER current density (70 mA/cm^2) than the commercial IrO_2 NPs (58 mA/cm^2) at 0.6 V versus Ag/AgCl electrode in deaerated 0.5 M KOH electrolyte. In 0.5 M KOH electrolyte saturated with O_2, the OER current density of the IrO_2 NRs and IrO_2 NPs were found to be 71 mA/cm^2 and 61 mA/cm^2, respectively. Moreover, in 0.5 M KOH deaerated electrolyte, the HER current density of the IrO_2 NRs (25 mA/cm^2) was found to be nearly double to that of the commercial IrO_2 NPs (14 mA/cm^2). These current densities are comparable with, and in most cases, higher than reported results in the literature, while the synthesis method employed here for these IrO_2 NRs is much more facile, cost-efficient and environmentally-friendly.

Acknowledgment

The authors thank the support from the Air Force Office of Scientific Research (award # FA9550-12-1-0159), USDA National Institute of Food and Agriculture HSI Collaboration: Integrating Food Science/Engineering and Education Network (IFSEEN, award number: 2015-38422-24059), and the National Science Foundation under DMR grant # 1523577 (PREM: UTRGV-UMN Partnership for Fostering Innovation by Bridging Excellence in Research and Student Success). J.A. is gratefully acknowledged "The Deanship of Scientific Research, Research Center, College of Science, King Saud University, Kingdom of Saudi Arabia. The authors also thank to Mr. Q. Li for taking SEM images and Ms. J. Cruz for performing BET measurements.

References

[1] C.H. Chang, T.S. Yuen, Y. Nagao, H. Yugami, Electrocatalytic activity of iridium oxide nanoparticles coated on carbon for oxygen reduction as cathode catalyst in polymer electrolyte fuel cell, Journal of Power Sources 195 (18) (2010) 5938–5941.
[2] W. Yao, J. Yang, J. Wang, Y. Nuli, Chemical deposition of platinum nanoparticles on iridium oxide for oxygen electrode of unitized regenerative fuel cell, Electrochemistry Communications 9 (5) (2007) 1029–1034.
[3] F.A. Frame, T.K. Townsend, R.L. Chamousis, E.M. Sabio, T. Dittrich, N.D. Browning, F.E. Osterloh, Photocatalytic water oxidation with nonsensitized IrO_2 nanocrystals under visible and UV light, Journal of the American Chemical Society 133 (19) (2011) 7264–7267.
[4] J. Tang, B. Kong, Y. Wang, M. Xu, Y. Wang, H. Wu, G. Zheng, Photoelectrochemical detection of glutathione by IrO_2–Hemin–TiO_2 nanowire arrays, Nano Letters 13 (11) (2013) 5350–5354.
[5] S.D. Tilley, M. Cornuz, K. Sivula, M. Grätzel, Light-induced water splitting with hematite: improved nanostructure and iridium oxide catalysis, Angewandte Chemie International Edition 49 (36) (2010) 6405–6408.
[6] W.J. Youngblood, S.-H.A. Lee, Y. Kobayashi, E.A. Hernandez-Pagan, P.G. Hoertz, T.A. Moore, A.L. Moore, D. Gust, T.E. Mallouk, Photoassisted overall water splitting in a visible light-absorbing dye-sensitized photoelectrochemical cell, Journal of the American Chemical Society 131 (3) (2009) 926–927.
[7] C. Zhao, Y. E., L. Fan, Enhanced electrochemical evolution of oxygen by using nanoflowers made from a gold and iridium oxide composite, Microchimica Acta 178 (1-2) (2012) 107–114.
[8] P.G. Hoertz, Y.-I. Kim, W.J. Youngblood, T.E. Mallouk, Bidentate dicarboxylate capping groups and photosensitizers control the size of IrO_2 nanoparticle catalysts for water oxidation, The Journal of Physical Chemistry B 111 (24) (2007) 6845–6856.
[9] J. Cheng, H. Zhang, H. Ma, H. Zhong, Y. Zou, Study of carbon-supported IrO_2 and RuO_2 for use in the hydrogen evolution reaction in a solid polymer electrolyte electrolyzer, Electrochimica Acta 55 (5) (2010) 1855–1861.
[10] Y. Lee, J. Suntivich, K.J. May, E.E. Perry, Y. Shao-Horn, Synthesis and activities of rutile IrO_2 and RuO_2 nanoparticles for oxygen evolution in acid and alkaline solutions, The Journal of Physical Chemistry Letters 3 (3) (2012) 399–404.
[11] R.D.L. Smith, B. Sporinova, R.D. Fagan, S. Trudel, C.P. Berlinguette, Facile photochemical preparation of amorphous iridium oxide films for water oxidation catalysis, Chemistry of Materials 26 (2014) 1654–1659.
[12] K.A. Stoerzinger, L. Qiao, M.D. Biegalski, Y. Shao-Horn, Orientation-dependent oxygen evolution activities of rutile IrO_2 and RuO_2, The Journal of Physical Chemistry Letters 5 (10) (2014) 1636–1641.
[13] C. Zhao, H. Yu, Y. Li, X. Li, L. Ding, L. Fan, Electrochemical controlled synthesis and characterization of well-aligned IrO_2 nanotube arrays with enhanced electrocatalytic activity toward oxygen evolution reaction, Journal of Electroanalytical Chemistry 688 (2013) 269–274.
[14] S. Siracusano, V. Baglio, A. Stassi, R. Ornelas, V. Antonucci, A.S. Aricò, Investigation of IrO_2 electrocatalysts prepared by a sulfite-couplex route for the O_2 evolution reaction in solid polymer electrolyte water electrolyzers, International Journal of Hydrogen Energy 36 (13) (2011) 7822–7831.
[15] E. Mayousse, F. Maillard, F. Fouda-Onana, O. Sicardy, N. Guillet, Synthesis and characterization of electrocatalysts for the oxygen evolution in PEM water electrolysis, International Journal of Hydrogen Energy 36 (17) (2011) 10474–10481.
[16] V.K. Puthiyapura, S. Pasupathi, H. Su, X. Liu, B. Pollet, K. Scott, Investigation of supported IrO_2 as electrocatalyst for the oxygen evolution reaction in proton exchange membrane water electrolyser, International Journal of Hydrogen Energy 39 (5) (2014) 1905–1913.
[17] J.C. Cruz, V. Baglio, S. Siracusano, R. Ornelas, L. Ortiz-Frade, L.G. Arriaga, V. Antonucci, A.S. Aricò, Nanosized IrO_2 electrocatalysts for oxygen evolution reaction in an SPE electrolyzer, Journal of Nanoparticle Research 13 (4) (2011) 1639–1646.
[18] A.A. Gambardella, S.W. Feldberg, R.W. Murray, Electron transfer dynamics of iridium oxide nanoparticles attached to electrodes by self-assembled monolayers, Journal of the American Chemical Society 134 (13) (2012) 5774–5777.
[19] S. Cherevko, T. Reier, A.R. Zeradjanin, Z. Pawolek, P. Strasser, K.J.J. Mayrhofer, Stability of nanostructured iridium oxide electrocatalysts during oxygen evolution reaction in acidic environment, Electrochemistry Communications 48 (2014) 81–85.
[20] K. Kadakia, M.K. Datta, O.I. Velikokhatnyi, P.H. Jampani, P.N. Kumta, Fluorine doped (Ir,Sn,Nb)O_2 anode electro-catalyst for oxygen evolution via PEM based water electrolysis, International Journal of Hydrogen Energy 39 (2) (2014) 664–674.
[21] Z.-P. Liu, S.J. Jenkins, D.A. King, Role of nanostructured dual-oxide supports in enhanced catalytic activity: theory of CO oxidation over Au/IrO_2/TiO_2, Physical Review Letters 93 (15) (2004) 156102.
[22] X.-H. Jian, D.-S. Tsai, W.-H. Chung, Y.-S. Huang, F.-J. Liu, Pt-Mo electrodeposited onto Ir-IrO_2 nanorods and their catalytic activities in methanol and ethanol oxidation, Journal of Materials Chemistry 19 (11) (2009) 1601–1607.
[23] T.W. Chao, C.J. Liu, A.H. Hsieh, H.M. Chang, Y.S. Huang, D.S. Tsai, Quartz crystal microbalance sensor based on nanostructured IrO_2, Sensors and Actuators B: Chemical 122 (1) (2007) 95–100.
[24] Z.G. Chen, F. Pei, Y.T. Pei, J.T.M. De Hosson, A versatile route for the synthesis of single crystalline oxide nanorods: growth behavior and field emission characteristics, Crystal Growth & Design 10 (6) (2010) 2585–2590.
[25] Y.M. Chen, C.A. Chen, Y.S. Huang, K.Y. Lee, K.K. Tiong, Synthesis of IrO_2 nanocrystals on carbon nanotube bundle arrays and their field emission characteristics, Journal of Alloys and Compounds 487 (1–2) (2009) 659–664.
[26] K. Huang, Y. Li, Y. Xing, Increasing round trip efficiency of hybrid Li–air battery with bifunctional catalysts, Electrochimica Acta 103 (0) (2013) 44–49.
[27] S.A. Mahmoud, S.M. Al-Shomar, A.A. Akl, Electrical characteristics and nanocrystalline formation of sprayed iridium oxide thin films, Advances in Condensed Matter Physics 2010 (2010).
[28] C.A. Chen, Y.M. Chen, Y.S. Huang, D.S. Tsai, P.C. Liao, K.K. Tiong, Synthesis and structural characterization of twinned V-shaped IrO_2 nanowedges on TiO_2 nanorods via MOCVD, Journal of Alloys and Compounds 480 (1) (2009) 107–110.
[29] C.A. Chen, Y.M. Chen, Y.S. Huang, D.S. Tsai, K.K. Tiong, C.H. Du, Growth and characterization of V-shaped IrO_2 nanowedges via metal-organic vapor deposition, Nanotechnology 19 (46) (2008) 465607.
[30] R.S. Chen, Y.S. Chen, Y.S. Huang, Y.L. Chen, Y. Chi, C.S. Liu, K.K. Tiong, A.J. Carty, Growth of IrO_2 films and nanorods by means of CVD: an example of compositional and morphological control of nanostructures, Chemical Vapor Deposition 9 (6) (2003) 301–305.
[31] R.S. Chen, Y.S. Huang, Y.M. Liang, D.S. Tsai, K.K. Tiong, Growth and characterization of iridium dioxide nanorods, Journal of Alloys and Compounds 383 (1–2) (2004) 273–276.
[32] R.-S. Chen, Y.-S. Huang, Y.-M. Liang, D.-S. Tsai, Y. Chi, J.-J. Kai, Growth control and characterization of vertically aligned IrO_2 nanorods, Journal of Materials Chemistry 13 (10) (2003) 2525–2529.

[33] G. Wang, D.-S. Tsai, Y.-S. Huang, A. Korotcov, W.-C. Yeh, D. Susanti, Selective growth of IrO_2 nanorods using metalorganic chemical vapor deposition, Journal of Materials Chemistry 16 (8) (2006) 780–786.
[34] C. Reui-San, C. Hung-Min, H. Ying-Sheng, T. Dah-Shyang, C. Kuan-Cheng, Morphological evolution of the self-assembled IrO_2 one-dimensional nanocrystals, Nanotechnology 16 (1) (2005) 93.
[35] Y. Lee, M. Kang, J.H. Shim, N.-S. Lee, J.M. Baik, Y. Lee, C. Lee, M.H. Kim, Growth of highly single crystalline IrO_2 nanowires and their electrochemical applications, The Journal of Physical Chemistry C 116 (34) (2012) 18550–18556.
[36] B.C. Satishkumar, A. Govindaraj, M. Nath, C.N.R. Rao, Synthesis of metal oxide nanorods using carbon nanotubes as templates, Journal of Materials Chemistry 10 (9) (2000) 2115–2119.
[37] A. Korotcov, H.-P. Hsu, Y.-S. Huang, D.-S. Tsai, Raman scattering characterization of well-aligned IrO_2 nanocrystals grown on sapphire substrates via reactive sputtering, Journal of Raman Spectroscopy 37 (12) (2006) 1411–1415.
[38] S. Ardizzone, C. Bianchi, L. Borgese, G. Cappelletti, C. Locatelli, A. Minguzzi, S. Rondinini, A. Vertova, P. Ricci, C. Cannas, A. Musinu, Physico-chemical characterization of IrO_2-SnO_2 sol-gel nanopowders for electrochemical applications, Journal of Applied Electrochemistry 39 (11) (2009) 2093–2105.
[39] G. Wang, F. Cheng, Y. Yu, C. Liang, T. Xu, M. Pan, SC-IrO_2 NR-carbon hybrid: a catalyst with high electrochemical stability for oxygen reduction, Science China Chemistry 56 (1) (2013) 131–136.
[40] Y. Mao, Facile molten-salt synthesis of double perovskite La_2BMnO_6 nanoparticles, RSC Advances 2 (33) (2012) 12675–12678.
[41] Y. Mao, X. Guo, J.Y. Huang, K.L. Wang, J.P. Chang, Luminescent nanocrystals with $A_2B_2O_7$ composition synthesized by a kinetically modified molten salt method, The Journal of Physical Chemistry C 113 (4) (2009) 1204–1208.
[42] H. Zhou, Y. Mao, S.S. Wong, Probing structure-parameter correlations in the molten salt synthesis of $BaZrO_3$ perovskite submicrometer-sized particles, Chemistry of Materials 19 (22) (2007) 5238–5249.
[43] I. Taurino, S. Carrara, M. Giorcelli, A. Tagliaferro, G. De Micheli, Comparison of two different carbon nanotube-based surfaces with respect to potassium ferricyanide electrochemistry, Surface Science 606 (3–4) (2012) 156–160.
[44] S. Min-Jung, Y. Dong-Hwa, J. Joon-Hyung, M. Nam-Ki, H. Suk-In, Comparison of effective working electrode areas on planar and porous silicon substrates for cholesterol biosensor, Japanese Journal of Applied Physics 45 (9R) (2006) 7197.
[45] A.A.A. Aljabali, J.E. Barclay, J.N. Butt, G.P. Lomonossoff, D.J. Evans, Redox-active ferrocene-modified Cowpea mosaic virus nanoparticles, Dalton Transactions 39 (32) (2010) 7569–7574.
[46] K. Yoon, Y. Cho, D. Kang, Molten salt synthesis of lead-based relaxors, Journal of Materials Science 33 (12) (1998) 2977–2984.
[47] P.M. Rørvik, T. Lyngdal, R. Sæterli, A.T.J. van Helvoort, R. Holmestad, T. Grande, M.-A. Einarsrud, Influence of volatile chlorides on the molten salt synthesis of ternary oxide nanorods and nanoparticles, Inorganic Chemistry 47 (8) (2008) 3173–3181.
[48] W. Wang, C. Xu, X. Wang, Y. Liu, Y. Zhan, C. Zheng, F. Song, G. Wang, Preparation of SnO_2 nanorods by annealing SnO_2 powder in NaCl flux, Journal of Materials Chemistry 12 (6) (2002) 1922–1925.
[49] W.Z. Wang, C.K. Xu, G.H. Wang, Y.K. Liu, C.L. Zheng, Preparation of smooth single-crystal Mn_3O_4 nanowires, Advanced Materials 14 (11) (2002) 837–840.
[50] Z. Cai, X. Xing, R. Yu, X. Sun, G. Liu, Morphology-controlled synthesis of lead titanate powders, Inorganic Chemistry 46 (18) (2007) 7423–7427.
[51] Y. Mao, S. Banerjee, S.S. Wong, Large-Scale Synthesis of single-crystalline perovskite nanostructures, Journal of the American Chemical Society 125 (51) (2003) 15718–15719.
[52] V.V. Gorodetskii, V.A. Neburchilov, Tantalum oxide effect on the surface structure and morphology of the IrO_2 and $IrO_2 + RuO_2 + TiO_2$ coatings and on the corrosion and electrochemical properties of anodes prepared from these, Russian Journal of Electrochemistry 43 (2) (2016) 223–228.
[53] L. Ouattara, S. Fierro, O. Frey, M. Koudelka, C. Comninellis, Electrochemical comparison of IrO_2 prepared by anodic oxidation of pure iridium and IrO_2 prepared by thermal decomposition of H_2IrCl_6 precursor solution, Journal of Applied Electrochemistry 39 (8) (2009) 1361–1367.
[54] J. Ahmed, P. Trinh, A.M. Mugweru, A.K. Ganguli, Self-assembly of copper nanoparticles (cubes, rods and spherical nanostructures): Significant role of morphology on hydrogen and oxygen evolution efficiencies, Solid State Sciences 13 (5) (2011) 855–861.
[55] D. Owens, A. Han, L. Sun, Y. Mao, Synthesis of VTMS(X)-HMS-3 Mesoporous Ordered Silica for Hydrogen Storage, International Journal of Hydrogen Energy (2015) 40 in press.
[56] J.C.F. Boodts, S. Trasatti, Hydrogen evolution on iridium oxide cathodes, Journal of Applied Electrochemistry 19 (2) (1989) 255–262.